Microbricks for Three-Dimensional Reconfigurable Modular Microsystems

Jonathan D. Hiller, Joseph Miller, and Hod Lipson, *Member, IEEE*

Abstract—This paper explores the design of "microbricks"—interlocking microscale building blocks that can be used to assemble and reconfigure 3-D structures on a regular lattice. We present the design and fabrication of a space-filling rotation and flip-invariant 500-μm microbrick architecture suitable for 3-D assembly. We describe the design considerations used to optimize mechanical, fabrication, and assembly properties of the components and the finished structures. The final brick geometry was fabricated using two different fabrication techniques: Silicon bricks were micromachined out of silicon, and SU-8 polymer tiles were built up in a three-layer process. The resulting bricks were characterized, and proof-of-concept structures comprising ten bricks were assembled to demonstrate the physical interlocking and compatibility between the two materials. We suggest that the presented interlocking geometry could serve in the future to fabricate passive and active modular macroscale structures from microscale components. **[2011-0024]**

Index Terms—Integrated systems, microbrick, modular architecture, rapid assembler.

I. INTRODUCTION

MODULAR architectures comprising functional components with standard interfaces have been recognized as a key to the growth in complexity in microelectronic systems [1]–[3]. Mechanical systems and components, however, have largely resisted standardization, thus hindering the ability to quickly assemble complex systems out of standardized components. One challenge to realizing 3-D modular microsystem architectures is the identification of a basic mechanical building block. Once such a module is designed, it can be fabricated of various materials in independent processes. Both passive and functionalized bricks can be simulated, fabricated, and assembled, spanning a large design space of potential integrated systems.

Once a standardized interface between microbricks is defined, the fabrication methods and functional complexity of each individual brick are decoupled from the final assembly process. This allows for a compatible industry-wide infrastructure to develop around a given microbrick architecture, enabling exponential growth of complexity. Unlike the analogous Moore's law, which defines the growth of the semiconductor industry by the exponentially decreasing transistor size, the analogous scaling law for the microbrick industry would describe the exponentially increasing design space reachable in multiple physical domains.

A number of systems have explored the use of modular interlocking components [4], [5]. While these systems are inherently serial in their assembly, they demonstrate the feasibility of manipulating and assembling interlocking shapes at this scale [6]. However, the components used in these systems are not geared toward the assembly of general 3-D integrated structures. For example, they are porous, a property that is well suited for their use in tissue scaffolds, but could negatively affect the mechanical properties.

In this paper, we explore the considerations for the geometric design of a modular building block, based on mechanical properties, as well as fabrication constraints and assembly requirements. We do not consider electrical interconnectivity, although we have begun exploring this elsewhere [7].

II. BRICK DESIGN

A. Design Requirements

It quickly becomes evident that many competing objectives factor into the optimal design of the individual microbricks. Perhaps the most important tradeoff is between the geometric complexity of each brick and the complexity of mechanically connecting adjacent bricks. On the one hand, the geometry must be as simple as possible to facilitate ease of mass fabrication, yet the shapes must rigidly interlock in three dimensions to create structures [8]. The design requirements that we consider here for the microbricks are as follows:

1) physically interlocked in three dimensions;
2) simple geometry;
3) ease of alignment for assembly;
4) ease of fabrication in bulk;
5) mechanically robust.

Physically interlocking bricks are desirable over gluing or otherwise adhering adjacent bricks for several reasons. First, this decouples the material properties of the brick from the assembly process. This allows bricks to be composed of any solid material, even materials that are mutually incompatible in any given fabrication process. Second, each brick self-aligns with

its neighbors upon assembly, ensuring that a regular lattice with well-defined interfaces is preserved throughout the structure. This enables discrete (digital) feedback of the assembly process that would not be possible if continuous errors in position between adjacent bricks were possible. However, the result is that the need for physical interlocking in all three dimensions prohibits the possibility of using simple 2-D shapes that would be easier to manufacture.

Another tradeoff exists between the number of redundant orientations of a brick and the geometric complexity. If each brick must be actively aligned to a single correct orientation before assembly, there will be a large penalty in assembly complexity and efficiency. This problem can be mitigated in one of two ways. First, alignment can be maintained throughout the brick manufacturing, distributing, and assembly process. Although some brick manufacturing processes may allow the rotation and orientation to be maintained throughout the fabrication and assembly process [9], there are many brick fabrication processes where this would be prohibitive. For instance, when the substrate on which the bricks are manufactured on is costly and reusable, each microbrick would need to be transferred to an intermediate substrate while maintaining orientations.

Alternatively, to better meet the goals of a mass fabrication process, we propose that the microbrick geometry should be rotation and flip invariant. This allows the bricks to be manufactured, stored, and transported without regard to absolute orientation and then passively aligned in parallel for assembly. Because any possible incorrect brick orientations are eliminated by design, the assembly process becomes significantly more simple and robust.

Other important considerations that are critical to a successful microbrick architecture regard the scaling of structures from the tens of bricks presented here to objects composed of millions, billions, or even more microbricks. It quickly becomes apparent that not only will massively parallel assembly methods be required but also massively parallel microbrick manufacturing methods [10]. Ideally, the geometry would be naturally suitable for fabrication processes such as micromachining [11], hot embossing [12], [13], [14], microcasting [15], or additive layered manufacturing [16], [17]. All of these processes leverage reusable complexity, in which a single complex template with many individual brick templates is fabricated which can then be used to easily and repeatedly fabricate many bricks in parallel. Given this class of manufacturing methods, it is desirable for the objects to be 2.5-D or composed solely of extruded 2-D profiles in a single plane. In order to facilitate all of these manufacturing processes, there should be no internal or undercut surfaces that would prevent having a single parting plane for a mold.

Finally, the shape design of the individual bricks will have a large effect on the aggregate material properties of an object composed of many such bricks. Although a block of bricks made of a given material will never be as strong as a homogeneous block of this material in the same dimensions [18], the differences between the two can be minimized by a directed choice of brick geometry. In order to maximize the mechanical properties of the material, it is desirable that the bricks tile in 3-D space such that they are space filling. With such a system,

voids may still be introduced by leaving empty locations in the lattice in applications where weight savings or porosity is desirable.

B. Brick Geometry

To begin the discussion of selecting a brick geometry, we first broadly consider the space-filling requirement presented earlier. There are a finite number of tessellation modes that fill 3-D space. Of these, there are 3-D tessellating shapes based on platonic solids and 2.5-D extrusions of 2-D shapes that also fill 3-D space. Although cubes are the only 3-D platonic solid that tiles directly in euclidean space [19], truncating tetrahedra and octahedra can also fill euclidean space [8]. 2.5-D tessellating shapes such as equilateral triangles, rectangles, and hexagons tessellate in two dimensions to form a complete layer, and then, subsequent layers may be stacked to achieve a 3-D lattice.

For both the 3-D and 2.5-D tiling shapes, geometry must be added at some or all of the interfaces to enable interlocking. If care is taken, this can be done with no loss of possible brick orientations, thereby maximizing the rotation and flip invariance. If the layers are suitably offset laterally from each other in the layer-based 2.5-D schemes, a rigid structure can be created by interlocking only between bricks of adjacent layers and not between adjacent bricks in the same layer. This allows a much simpler design while also allowing bricks within a given layer to be assembled in any order, even simultaneously in a parallel assembly process.

For these reasons, 2.5-D square interlocking tiles were selected for fabrication due to the ease of assembly and maximum degrees of rotation and flip invariance. Offset between layers was logically selected to be half a tile dimension in both lateral axes to allow for maximal redundancy and interconnection area. The simplest interlocking scheme between bricks in adjacent layers could be achieved using a simple peg-and-hole design, but when mechanical characteristics are considered, it quickly becomes apparent that more mechanically robust designs are possible.

An improved design (see Fig. 1) was developed that minimizes both the geometrical complexity of the tile and the internal stress concentrations as the tile is physically loaded. The chosen microbrick design has eight redundantly identical orientations and no "partially correct" orientations that could cause problems in a passive alignment process. The geometry consists of a ring structure into which 4 ft of the four adjoining bricks in the next layer presses. Each foot sticks up approximately 1/4 of the total height H [see Fig. 1(a)]. Thus, when feet are inserted into a given brick from both above and below, they touch in the middle, yielding a space-filling design.

Given the constraint of filling 3-D space, there were four parameters to vary: the tile edge dimension (D), the tile height (H), the tab width (L), and the tab interface angle (A). All other dimensions are derived from these to satisfy the space-filling criterion. The tile edge dimension was selected to be 500 μm based on the desired scale of the bricks. 500-μm tiles are small enough that a structure composed of many such tiles would appear smooth to the human eye, yet large enough to be manipulated by hand when necessary. The tile height
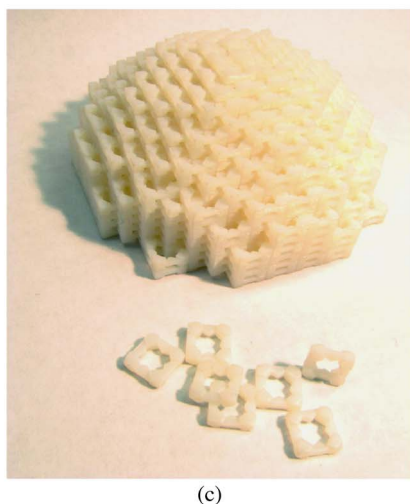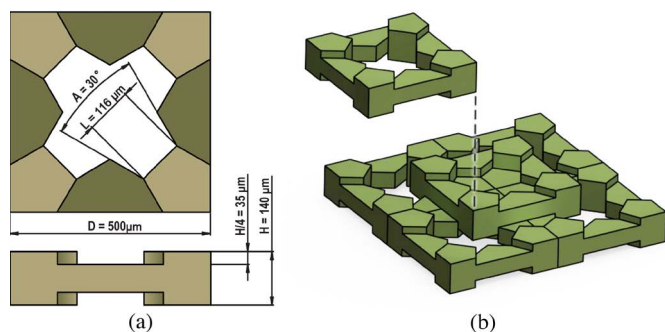
Fig. 1. Selected square tile design is (a) 500 μm square and 140 μm thick. The tab angle A was selected to be 30° with a tab width of 116 μm. The space-filling tiles interlock by offsetting each layer by 1/2 a tile dimension in X and Y. Millimeter-scale mock-ups assembled into a hemisphere demonstrate (c) a large-scale assembly.
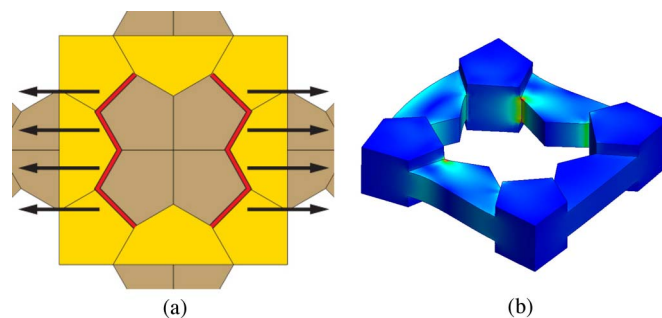

Fig. 2. (a) Tiles were loaded in simulation in a manner consistent with the forces that an individual tile would undergo when a larger structure is subjected to an axial tension load. An example output of the finite-element simulation shows the exaggerated deformation and stress concentrations resulting from the loading.

of 130 μm was selected as a compromise between the two manufacturing processes that were pursued to fabricate the bricks. The polymer bricks were built up from layers of SU-8 photoresist in an additive process. Given the relative difficulty of spinning very accurate and thick layers of SU-8 and the processing difficulty of aligning a large number of separate SU-8 layers, the geometry was kept as thin as possible. On the other hand, the silicon bricks were created with a subtractive process. Since the initial thickness of the wafer dictated the height (H) of the bricks, there were constraints on the thinnest possible wafer that could be reasonably handled. The 130-μm thickness was an appropriate compromise between manipulating silicon wafers that were thick enough to handle while not necessitating unreasonably thick SU-8 layers.

The other two free parameters dictate the size and shape of the tab feet and, by extension, the size and shape of the ring geometry. The tab width L was selected to be 116 μm as a starting point. Then, the brick geometry was analyzed to determine the optimal tab interface angle A. There are many arbitrary metrics that could be used to decide the best geometry. Here, we chose to use a combination of two metrics to capture information about the geometric complexity of the shape along with an estimate of how strong a structure composed of such microbricks would be.

The first metric was a measure of the compactness of a 3-D shape. Here, we define compactness as the total surface area of

the brick divided by the total volume of the brick. In this case, the total volume of the brick was constant due to the space-filling constraints. Essentially, varying the tab dimensions adds and subtracts equal quantities of material at different locations of the brick shape. Bricks with higher surface area are less compact and thus less desirable.

The second metric for each candidate brick geometry was obtained by performing finite-element analysis to approximate the tile's behavior in a lattice of tiles under tensile load. The axial tension scenario was selected as a worst case scenario because the space-filling nature of the bricks will give them favorable compressive properties as compared to tensile properties. The tiles were loaded as shown in Fig. 2(a), which is a good approximation of the forces that a tile will undergo within a structure under axial tension. One interface surface was fixed while the other had unit force applied in the outward direction. A linear elastic simulation was used with a mesh of approximately 230 000 elements. A sample output of the simulation is shown in Fig. 2(b). The maximum stress was output and normalized by the stiffness of the material used by the simulation to obtain a dimensionless qualitative indicator of the strength of each geometry. Due to the variation of meshes between geometries and the sensitivity of finite-element simulations to the mesh structure at sharp corners of a stress concentration, a line of best fit was calculated to the data using the least squares method with respect to the tab interface angle.

To obtain a single metric from the complexity and strength metrics, each unitless metric was normalized, and then, the two values were added to obtain the final geometry metric. The results of this analysis are shown in Fig. 3 for tab angles varying from 0° to 90°. The optimal design at the minimum of the curve was found to be very close to 30° with favorable overall properties. The final step before generating masks for the microfabrication processes was to include a 5-μm offset between all mating surfaces to mitigate concerns that the brittle tiles would fracture upon assembly.

III. BRICK MANUFACTURING

A. SU-8 Polymer Bricks

Standard photolithography techniques were used to create MicroChem SU-8 polymer microbricks. SU-8 is an ideal
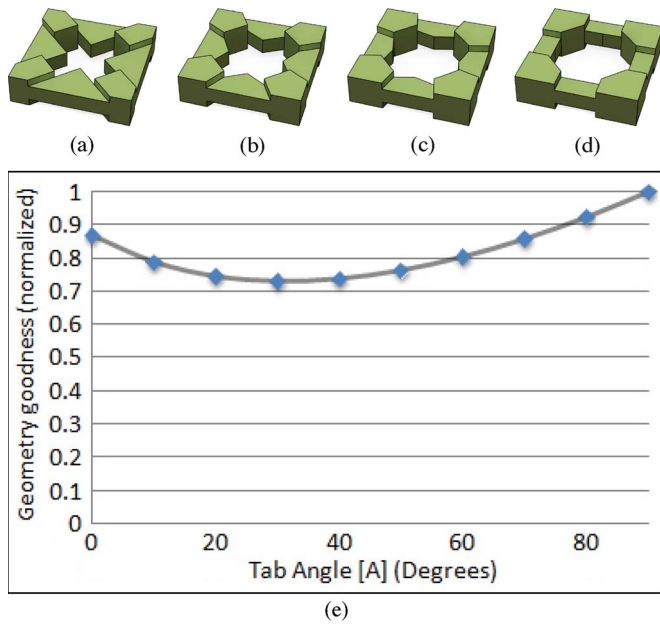
(a) (b) (c) (d)

(e)

Fig. 3. Interface angle of the tabs was optimized based on a combination of minimizing the total surface area of the tile and minimizing the internal stress when stacked microtiles are put under lateral load. Tab angles of (a) 0°, (b) 30°, (c) 60°, and (d) 90° illustrate the range of geometries under consideration. The optimal angle was determined to be 30°, which corresponds to a relative compact shape that performs well under mechanical loading.

TABLE I
SUMMARY OF MEASURED TILE DIMENSIONS. DIMENSIONS AND
STANDARD ERRORS ARE BASED ON MEASUREMENTS OF TEN TILES

	Silicon		SU-8	
	Dimension	StdErr	Dimension	StdErr
Tile Width	$497.08\mu m$	$0.14\mu m$	$500.75\mu m$	$0.13\mu m$
Total Thickness	$113.39\mu m$	$0.21\mu m$	$153.65\mu m$	$0.53\mu m$
Center Layers Thickness	$56.35\mu m$	$0.18\mu m$	$75.53\mu m$	$0.34\mu m$

involving a closed bowl spin of 500 r/min for 10 s followed by 3000 r/min for 30 s, with accelerations of 1000 r/s. The sequence was completed with an uncovered continuous spin of 1000 r/min to facilitate the edge bead removal. During this final stage, a SU-8 remover solvent was applied for 15 s at a distance of 10 mm from the edge of the wafer followed by a sweeping application starting outside the edge of the wafer and then moving inward until 8 mm from the edge of the wafer. The wafer was then allowed to continue spinning uncovered for 60 s to enable uniform solvent evaporation.

The wafer was then soft baked and exposed with a bottom side soft contact alignment. A filter was used to eliminate light below a 350-nm wavelength to prevent flawed exposure and rough edges of the SU-8. The wafer was then placed on the hot plate for a postbake. A longer hotter postbake (30 min at 95 °C) is required to help cross-link the exposed SU-8 and remove as much remaining solvent in the SU-8 as possible. This is crucial to provide a stable substrate for the remaining process steps since the unexposed SU-8 must remain in place to provide a flat substrate for the next layers.

Because the tiles have overhanging regions by necessity of design, care must be taken when exposing subsequent layers so that no UV light can reach this first layer and cross-link any unexposed regions of SU-8. To this end, a UV-opaque metallic layer was deposited between the first and second SU-8 layers. Chrome was selected for this task. A thermal evaporation of 100 nm of chrome was applied at 4 Å/s and 10 kV. This slower chrome deposition rate yielded more favorable chrome layers than faster depositions.

The second and third layers of SU-8 were done in a similar manner to the first layer of SU-8, with appropriate adjustments to the spin schedule to attain a 70-μm center layer with the SU-8 2050. Once all layers were in place and exposed, the SU-8 was developed to remove the superficial supporting material. After rinsing the wafer with isopropyl alcohol (IPA), it was placed in a chrome etch bath for 90 s to remove the now-revealed chrome layer. Next, the wafer was dried and placed in another SU-8 developer bath to develop the bottom layer. The wafer was then rinsed with IPA and air dried to remove the unexposed SU-8 of the initial layer. To finally release the bricks from the substrate, the wafer is placed in an MF 321 developer (tetramethylammonium hydroxide) bath for approximately 30 min until the bricks are released from the Omnicoat layer. The bricks were then strained out of solution and set aside to dry for assembly. Complete SU-8 tiles are shown in Fig. 5. A pictorial process table is included in Appendix A

Although silicon is a more traditional material for micro-fabrication, fabricating free bricks out of silicon had its own

negative epoxy-based photoresist for this purpose for two reasons. First, high aspect ratio structures are routinely fabricated with excellent accuracy [20], [21]. Second, it has a relatively large thickness allowance [22] and is available in a wide range of viscosities. The 2.5-D design of the microtiles enabled the SU-8 tiles to be created with three layers of separately spun and exposed SU-8. Overexposure of underlying SU-8 was minimized by masking the first layer with a vacuum-deposited metal layer. Process details are detailed hereinafter.

Before any layers of SU-8 were deposited, alignment marks were etched on the bottom side of the wafer to provide a reference to keep subsequent layers in proper alignment. SC 1827 photoresist was spun for 30 s at 2000 r/min on the underside of the wafer, prebaked for 1 min at 115 °C, and passively cooled to room temperature. A generic alignment mark photomask was used to expose the wafer for 15 s, and then, the wafer was developed normally. Twelve loops in a Uniaxis plasma etcher resulted in alignment marks etched approximately 4.8 μm deep, which was sufficient to be visible in subsequent alignment steps. The wafer was then stripped clean of the remaining photoresist.

In order to facilitate the removal of the SU-8 tiles from the wafer substrate, a sacrificial layer of MicroChem Omnicoat was first deposited. To ensure the reliable release of the finished bricks, it was found that this layer should be no less than 17 nm thick. After the layer was spun, the wafer was placed on a hot plate for 1 min at 200 °C to harden and then passively cooled to room temperature.

SU-8 2020 was selected for the thinner bottom and top layers in order to achieve the desired 35-μm layer thickness. SU-8 2050 was used for the thicker 70-μm center layer. For the 30-μm layers, the wafer was subjected to a spin process
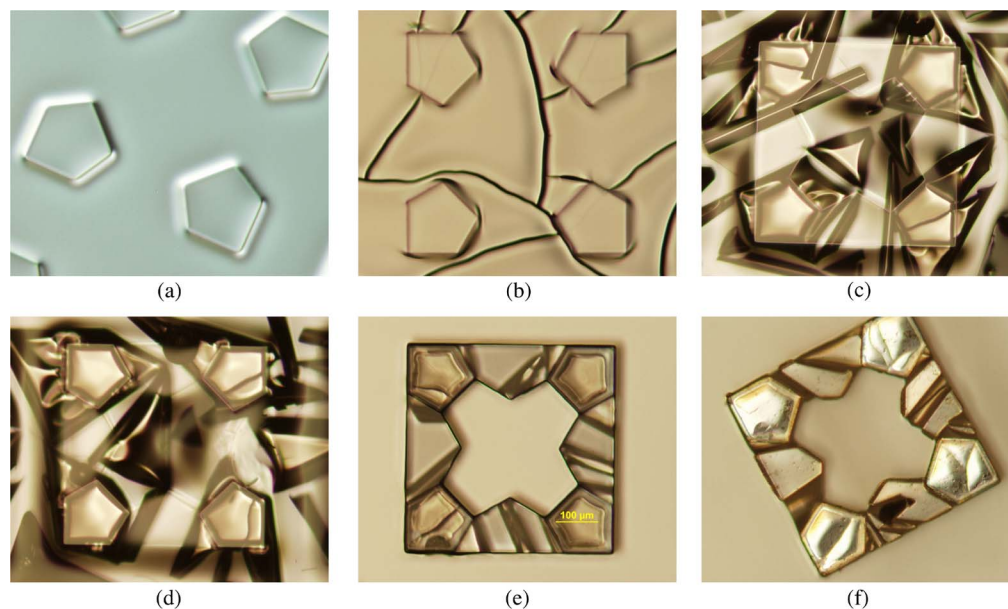
Fig. 4. Process of creating SU-8 microbricks. (a) First layer of SU-8 was deposited over a sacrificial layer, exposed, and baked. (b) Chrome layer masked the first SU-8 layer from being further cross-linked in later steps. Then, (c) the second and (d) the third layer of SU-8 were spun, exposed, and baked. (e) Top layers of SU-8 were then developed away, and the tiles were placed in a chrome etch to remove excess regions of the chrome layer. Then, the final layer of SU-8 was developed away, and the sacrificial layer was etched away, leaving free tiles.

challenges. Given that the target brick thickness was approximately 130 μm thick, the silicon bricks were fabricated by two-sided etching of a thin silicon wafer. Normal silicon wafers were first commercially ground to the correct thickness. Each side of the brick underwent two etching steps to reach the center plane of the wafer and impart the correct geometry.

To do a two-step silicon etch, a layer of SiO_2 was first deposited on one side of the wafer. This SiO_2 was then patterned to mask the area corresponding to the feet of the bricks. This was accomplished by masking with a positive photoresist and then reactive ion etching the surface to selectively remove the SiO_2. Then, another layer of photoresist was deposited over the patterned SiO_2. This layer was patterned and developed to leave the negative shape of the middle layer of the brick exposed. At this point, the exposed regions of the wafer were etched down by 35 μm with an inductively coupled plasma etcher utilizing the Bosch process for deep silicon etching. Then, the remaining layer of photoresist was stripped off, leaving only the previously patterned SiO_2 layer. Another 35-μm etch was done so that areas exposed for the first etch were now approximately 65 μm deep, corresponding to the approximate midplane of the wafer.

Before the same process could be completed from the opposite side to complete the brick geometry, a sacrificial membrane was deposited on the recently etched side to hold the bricks in place during the final silicon etching step from the other side. A combined layer of SiO_2 and nitride was deposited using plasma-enhanced chemical vapor deposition. The wafer was then flipped, and the two-layer etching process was repeated. The final etching step was allowed to continue until the silicon wafer was etched completely through in the exposed regions. The membrane holding the bricks together was then dissolved to leave the free bricks. A pictorial process table is included in Appendix B.

IV. RESULTS AND CONCLUSIONS

A. SU-8 Bricks

Overall, the SU-8 tiles displayed excellent feature accuracy in the horizontal plane. However, the SU-8 tiles ended up slightly thicker than the target dimension, although not detrimentally so. In the horizontal plane, the tiles were 0.75 μm large (see Table I). This is likely due to the mild bleeding of the UV at the edge of the mask, which cross-linked slightly more than the nominal amount of SU-8. The most difficult to control parameter in the SU-8 process was spinning an accurate thickness of the SU-8 layers. Based on the steps outlined earlier, the tiles ended up being 153 μm thick on average, which was slightly thicker than the target height of 140 μm. However, the relative thicknesses of the layers were very close to the desirable ratios, with the center layer being 49.2% of the total thickness (nominally 50%).

The main processing challenge of the SU-8 brick fabrication process was obtaining a suitable UV masking layer after the first SU-8 layer. This masking layer needed to be thick enough to successfully block light from penetrating and curing the SU-8 below, while not being so thick as to be brittle and crack. This, in turn, would also allow curing of the underlying SU-8 beneath the cracks. Even with the successful 100-nm chrome layer, this masking layer was observed to have a few minor ruptures [see Fig. 4(b)] after cooling from deposition. Subsequent steps in the fabrication process introduced dramatic wrinkling of the chrome layer, likely from the thermal stresses of baking and cooling the SU-8. However, UV bleeding was still kept to a minimum, as evidenced by the lack of unwanted cured SU-8 in Fig. 5(b).

Another option to mask the lower layer of SU-8 was to replace the chrome in the process with an aluminum layer. This yielded very smooth and effective masking layers that were not prone to cracking or wrinkling. However, aluminum is more
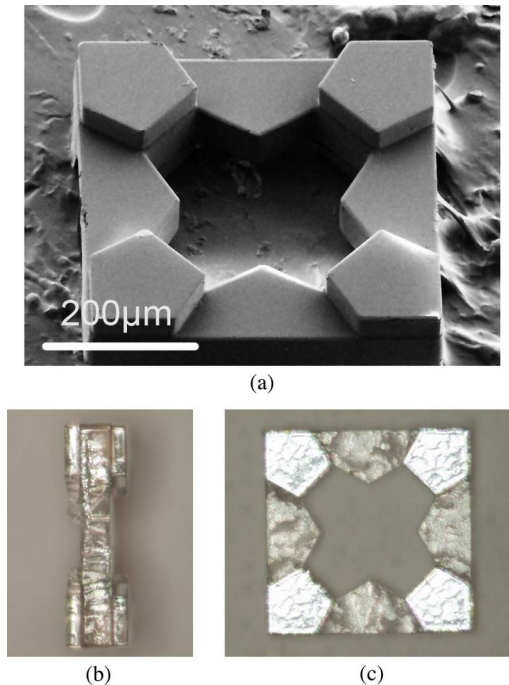
Fig. 5. Completed SU-8 microbricks. The SEM image shows (a) excellent feature accuracy. (b) Side and (c) top views show the individual layers of SU-8 clearly, as well as the finished aspect ratio of the tiles.

reactive than chrome to the SU-8 developing solution. This led to unwanted dissolving of the aluminum that holds the bottom of the feet to the rest of the tile. With these significant incuts between the first and second layers of SU-8, the tiles did not hold together well enough to assemble (see Figs. 6 and 7).

B. Silicon Bricks

In contrast to the SU-8 tiles, the silicon tiles ended up smaller than the target dimensions. In the horizontal plane, the tiles were 2.92 μm small (see Table I). This can likely be attributed to the plasma etching mildly undercutting the masked region. However, the wafers that were used in these experiments were on average only 113 μm thick, which gave the silicon bricks a significantly different aspect ratio than the SU-8 tiles. However, the relative thicknesses of the feet with respect to the thickness of the center layer were 49.7%, which was very close to the desired nominal 50%.

The challenges of fabricating the silicon bricks revolved around the use of very thin and fragile silicon wafers. Aside from needing extra care in all stages of processing, the correct proportions of SiO_2 and nitride for the retaining layer were critical. The retaining layer had to be tensile so that, as the final micrometers of silicon were etched away, the tiles would hold in the correct position. However, a tensile layer on one side of a very thin silicon wafer introduces unwanted stresses that would repeatedly shatter the wafer in the final stages of etching. To address this, the membrane was tuned to be only very slightly tensile by correctly proportioning SiO_2 and nitride.

C. Tile Assembly

In order to demonstrate the tiles interlocking in three dimensions, a proof-of-concept structure was assembled by hand from SU-8 bricks. The structure contains nine tiles in three layers and demonstrated the effectiveness of purely friction-based adhesion at the 500-μm scale rendering adhesives unnecessary. A SEM image is shown in Fig. 8(a), with a tenth tile unattached for reference. At 500 μm, the tiles can be manipulated by tweezers, although to assemble any significant number of tiles will necessitate further development of an automated system. Even though the SU-8 tiles were slightly on the large side, the surfaces were compliant enough to allow for assembly without undue breakage of the microbricks.

The silicon bricks, however, proved relatively fragile when pressed together, even though slightly undersized. This can be attributed to the relatively uncontrolled forces of assembling them by hand with tweezers. However, the more robust SU-8 tiles had enough compliance to assemble a structure that combined SU-8 and silicon tiles (see Fig. 9). Even though the aspect ratios were significantly different, they were still compatible with respect to the interlocking mechanism of feet fitting within the central ring.

V. CONCLUSION AND FUTURE WORK

Here, we have demonstrated the fabrication and assembling of a hybrid 3-D structure with both semiconductor and polymer components. The key to scaling up the complexity of microsystems lies in modularizing material and function, which requires standardizing the interface between components. In this way, each module type can be efficiently fabricated in independent optimized processes and then combined into a functional hybrid system. This enables materials and functions that would otherwise be mutually incompatible to be combined in a single integrated system. The first step in this process is to define a suitable mechanical module that is both robust and suitable for a massively parallel 3-D assembly process.

The mechanical architecture presented here fulfills these requirements. Components have simple 2.5-D geometric shapes that could be fabricated in bulk by a wide variety of common parallel microscale fabrication techniques. The bricks physically interlock yet can be assembled in a layer-by-layer process without complex 3-D alignment or manipulation. The bricks also maximize mechanical properties by utilizing a space-filling design and minimizing internal stress under tension.

There are many potential applications for 3-D multimaterial microbrick systems. Even with just two bricks of differing material stiffnesses, there are many possibilities for creating structures with novel properties [18]. Once modularity is enabled by well-defined interfaces between components, there are many ways to accelerate the design and assembly process. In the future, one can envision hierarchical assembly processes where individual components are assembled functional macrostructures which are then assembled into larger systems. Alternatively, more complex subsystems (e.g., a microcontroller component) could be prefabricated in a larger package such as a $3 \times 3 \times 3$ cube that is compatible with the smaller components or even with existing electrical interfaces.

In the distant future, we envision a library of compatible bricks spanning not only the range of properties of materials currently available to engineers but also incorporating specific
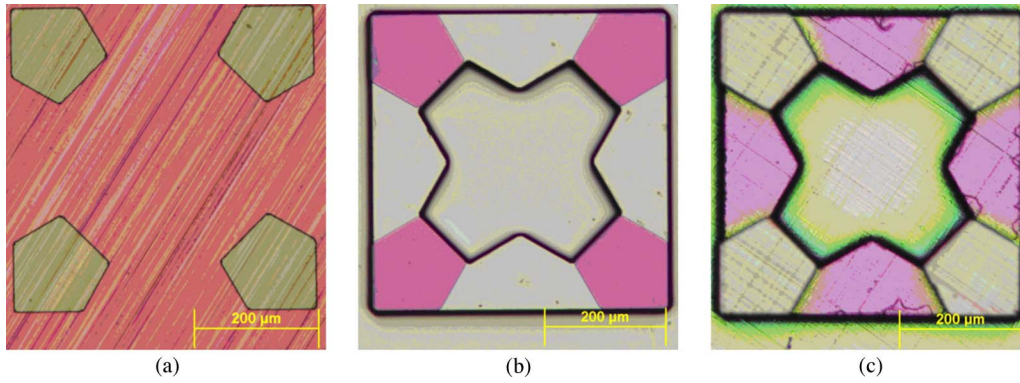
Fig. 6. Process of creating silicon microbricks. (a) Silicon wafer preground to the correct total brick thickness had SiO_2 deposited and etched to mask the second silicon etching process. (b) Then, another layer of photoresist was patterned, and the first silicon etching stage was completed, etching away the center and outside of each tile. (c) Then, the most recent layer of photoresist was stripped, and another silicon etching stage was completed, leaving the feet higher than the rest. A retaining membrane was then deposited on this side to hold the bricks in place while the process is completed from the opposite side.
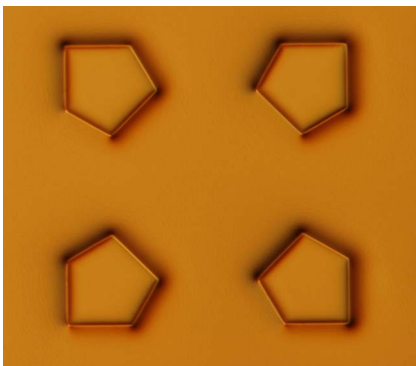

Fig. 7. Using aluminum instead of chrome [compare directly to Fig. 4(b)] in the SU-8 brick fabrication yielded less cracking, but aluminum reacted significantly with SU-8 developer which led to incutting of the tiles at the interface between the aluminum and the SU-8 in subsequent steps.
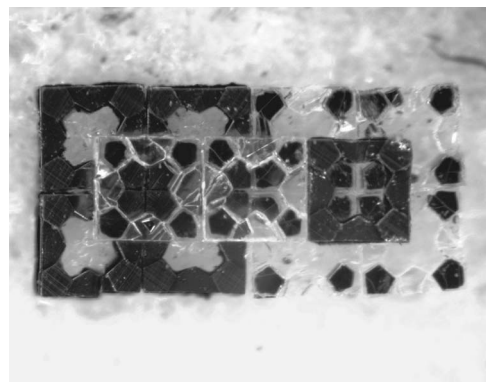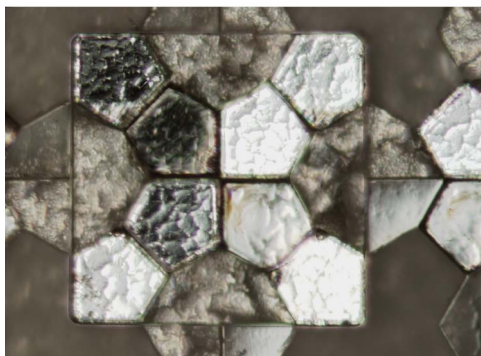

Fig. 9. Eleven-brick two-layer multimaterial structure was assembled by hand. Although the silicon bricks were too fragile to assemble on their own, combining them with the polymer bricks yielded a stable assembly. The dark tiles are silicon, while the light tiles are SU-8.

(a)

(b)

Fig. 8. Assembly of 500-μm tiles demonstrates a 3-D interlocking structure. (a) SEM image shows the whole structure, (b) while optical image shows the feet of the tiles in the lower layer inserted into the ring of the top voxel.
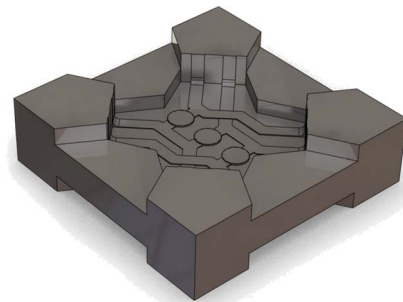
Fig. 10. Future microbricks will contain specific functionality. The internal part is not structural and therefore not considered in this analysis.

functionalities that would enable 3-D electromechanical objects to be fabricated quickly and cheaply from microbricks (see Fig. 10). This would allow for the exponential industry-wide growth of the complexity and functionality of multidomain microscale objects. Because of the reversible nature of the mechanical assembly, these objects could be just as easily decomposed back into individual tiles for reuse in other objects. In this way, the advantages of a modular architecture can be leveraged in the physical world to enable reconfigurable 3-D functional macroscale structures composed of microscale components.

APPENDIX A
SU-8 BRICK FABRICATION PROCESS DIAGRAMS

Step	Description	Diagram
1	Substrate patterned with sacrificial release layer	Omnicoat / Silicon Substrate
2	First layer of SU-8 is spun and patterned	Unexposed SU-8 / Omnicoat / Silicon Substrate
3	Masking chrome layer is deposited	Chrome / Unexposed SU-8 / Omnicoat / Silicon Substrate
4	Second layer of SU8 is deposited and patterned	Exposed SU-8 / Chrome / Unexposed SU-8 / Omnicoat / Silicon Substrate
5	Third layer of SU8 is deposited and patterned	Exposed SU-8 / Chrome / Unexposed SU-8 / Omnicoat / Silicon Substrate
6	SU-8, exposed chrome, and release layer are developed away	SU-8 / Silicon Substrate

APPENDIX B
SILICON BRICK FABRICATION PROCESS DIAGRAMS

Step	Description	Diagram
1	Silicon patterned with SiO$_2$	SiO2 / Silicon
2	Photoresist deposited and patterned	SiO2 / Resist / Silicon
3	First silicon etching step is performed	SiO2 / Resist / Silicon
4	Photoresist is stripped and second silicon etching step is performed	SiO2 / Silicon
5	Retaining layer of SiO$_2$ and nitride is deposited	SiO2 / SiO2+Nitride / Silicon
6	Process is repeated from the opposite side	SiO2 / SiO2+Nitride / Silicon / SiO2

ACKNOWLEDGMENT

REFERENCES

[1] E. Puik and L. van Moergestel, "Agile multi-parallel micro manufacturing using a grid of equiplets," in *Precision Assembly Technologies and Systems*, vol. 315, S. Ratchev, Ed. Boston, MA: Springer-Verlag, 2010, ser. IFIP Advances in Information and Communication Technology, pp. 271–282.

[2] A. Gutierrez, "Infrastructure driven strategies for microsystems business success in a market driven era," in *Proc. Commercial. Microsyst. Conf.*, San Diego, CA, Sep. 1998.

[3] A. Gutierrez, "MEMS/MST fabrication technology based on microbricks: A strategy for industry growth," *MST News*, vol. 1, no. 99, pp. 4–8, 1999.

[4] G. Skidmore, M. Ellis, A. Geisberger, K. Tsui, R. Saini, T. Huang, and J. Randall, "Parallel assembly of microsystems using Si micro electro mechanical systems," *Microelectron. Eng.*, vol. 67/68, no. 1, pp. 445–452, Jun. 2003.

[5] G. Skidmore, M. Ellis, A. Geisberger, K. Tsui, R. Saini, T. Huang, and J. Randall, "Parallel assembly of microsystems using Si micro electro mechanical systems," in *Proc. 28th Int. Conf. Micro-Nano-Eng.*, Lugano, Switzerland, 2002.

[6] H. Zhang, D. W. Hutmacher, F. Chollet, A. N. Poo, and E. Burdet, "Microrobotics and MEMS-based fabrication techniques for scaffold-based tissue engineering," *Macromolecular Biosci.*, vol. 5, no. 6, pp. 477–489, Jun. 2005.

[7] M. T. Tolley, A. Baisch, M. Krishnan, D. Erickson, and H. Lipson, "Interfacing methods for fluidically-assembled microcomponents," in *Proc. IEEE Int. Conf. Micro Electro Mech. Syst.*, Tucson, AZ, 2008, pp. 1073–1076.

[8] J. Hiller and H. Lipson, "Design and analysis of digital materials for physical 3D voxel printing," *Rapid Prototyping J.*, vol. 15, no. 2, pp. 137–149, 2009.

[9] H. Zhang, E. Burdet, A. Poo, and D. Hutmacher, "Microassembly fabrication of tissue engineering scaffolds with customized design," *IEEE Trans. Autom. Sci. Eng.*, vol. 5, no. 3, pp. 446–456, Jul. 2008.

[10] J. Hiller and H. Lipson, "Methods of parallel voxel manipulation for 3D digital printing," in *Proc. 18th Solid Freeform Fabrication Symp.*, 2007, pp. 200–211.

[11] M. Elwenspoek and H. V. Jansen, *Silicon Micromachining*. Cambridge, U.K.: Cambridge Univ. Press, 2004.

[12] H. Becker and U. Heim, "Hot embossing as a method for the fabrication of polymer high aspect ratio structures," *Sens. Actuators A, Phys.*, vol. 83, no. 1–3, pp. 130–135, May 2000.

[13] R. W. Jaszewski, H. Schift, J. Gobrecht, and P. Smith, "Hot embossing in polymers as a direct way to pattern resist," *Microelectron. Eng.*, vol. 41–42, pp. 575–578, Mar. 1998.

[14] R. W. Jaszewski, H. Schift, J. Gobrecht, and P. Smith, "Hot embossing in polymers as a direct way to pattern resist," in *Proc. Int. Conf. Micro-Nanofabrication*, Athens, Greece, 1997.

[15] L.-A. Liew, W. Zhang, V. M. Bright, L. An, M. L. Dunn, and R. Raj, "Fabrication of SiCN ceramic MEMS using injectable polymer-precursor technique," *Sens. Actuators A, Phys.*, vol. 89, no. 1/2, pp. 64–70, Mar. 2001.

[16] I. G. Foulds and M. Parameswaran, "A planar self-sacrificial multilayer SU-8-based MEMS process utilizing a UV-blocking layer for the creation of freely moving parts," *J. Micromech. Microeng.*, vol. 16, no. 10, p. 2109, Oct. 2006.

[17] A. Mata, A. J. Fleischman, and S. Roy, "Fabrication of multi-layer SU-8 microstructures," *J. Micromech. Microeng.*, vol. 16, no. 2, p. 276, Feb. 2006.

[18] J. Hiller and H. Lipson, "Tunable digital material properties for 3D voxel printers," *Rapid Prototyping J.*, vol. 16, no. 4, pp. 241–247, 2010.

[19] O. Delgado Friedrichs and D. H. Huson, "Tiling space by platonic solids, I," *Discrete Comput. Geometry*, vol. 21, no. 2, pp. 299–315, 1999.

[20] H. Lorenz, M. Despont, N. Fahrni, J. Brugger, P. Vettiger, and P. Renaud, "High-aspect-ratio, ultrathick, negative-tone near-UV photoresist and its applications for MEMS," *Sens. Actuators A, Phys.*, vol. 64, no. 1, pp. 33–39, Jan. 1998.

[21] H. Lorenz, M. Despont, N. Fahrni, J. Brugger, P. Vettiger, and P. Renaud, "High-aspect-ratio, ultrathick, negative-tone near-UV photoresist and its applications for MEMS," in *Proc. 10th IEEE Int. Workshop Micro Electro Mech. Syst.*, 1997, pp. 518–522.

[22] A. Bertsch, H. Lorenz, and P. Renaud, "3D microfabrication by combining microstereolithography and thick resist UV lithography," *Sens. Actuators A, Phys.*, vol. 73, no. 1/2, pp. 14–23, Mar. 1999.

Jonathan D. Hiller received the B.S. degree in mechanical engineering from the University of Washington, Seattle, in 2006, and the M.S. degree in mechanical engineering from Cornell University, Ithaca, NY, in 2009, where he is currently working toward the Ph.D. degree in the Cornell Computational Synthesis Laboratory.

He is a recipient of a National Science Foundation graduate research fellowship. His research interests are focused on the boundary between the physical and the digital world, specifically the automated design and fabrication of microbrick-based materials and systems.

Joseph Miller received the B.S. degree in physics from North Dakota State University, Fargo, ND, in 2010, where he is currently working toward the Ph.D. degree in the Materials and Nanotechnology Program.

He is currently working on a project involving the implementation of silicon quantum dots as a biological sensing device.

Hod Lipson (M'98) received the B.Sc. degree in mechanical engineering and the Ph.D. degree in mechanical engineering in computer-aided design and artificial intelligence in design from the Technion—Israel Institute of Technology, Haifa, Israel, in 1989 and 1998, respectively.

He is currently an Associate Professor with the Mechanical and Aerospace Engineering and Computing and Information Science Schools, Cornell University, Ithaca, NY. He was a Postdoctoral Researcher in the Department of Computer Science, Brandeis University, Waltham, MA. He was a Lecturer in the Department of Mechanical Engineering, Massachusetts Institute of Technology, Cambridge, where he was engaged in conducting research on design automation. His current research interests include computational methods to synthesize complex systems out of elementary building blocks and the application of such methods to design automation and their implication toward understanding the evolution of complexity in nature and in engineering.